Supporting Information

Environmentally Tolerant Multifunctional Eutectogel for Highly Sensitive Wearable Sensors

Zhengen Wei,[#a,b] Lianghao Jia[#a,b], Jinyu Yu[a,b], Hanrui Xu[a,b], Xing Guo[a,b], Tao Xiang[*a,b] and Shaobing Zhou[a,b]

Z. Wei, L. Jia, J. Yu, H. Xu, T. Xiang, and Prof. S. Zhou

Institute of Biomedical Engineering, College of Medicine, Southwest Jiaotong University, Chengdu 610031, China

School of Materials Science and Engineering, Southwest Jiaotong University, Chengdu 610031, China

E-mail: xita198906@swjtu.edu.cn, xita198906@163.com

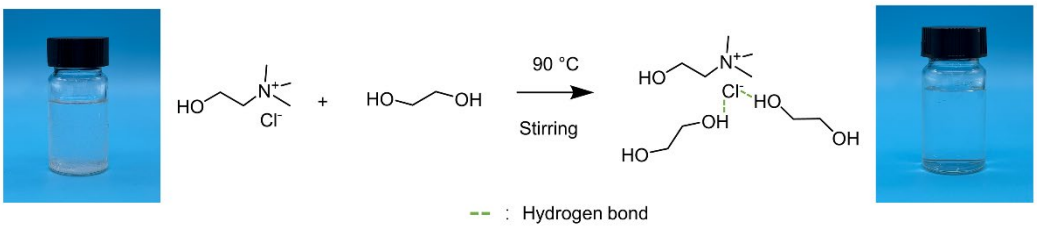

Fig. S1 Synthesis process of DES.

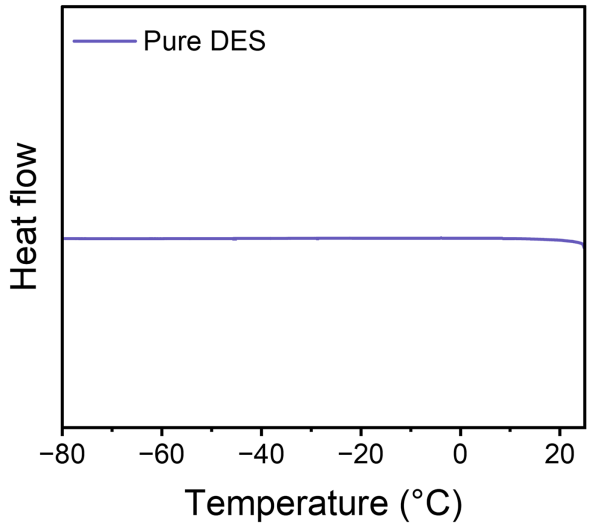

Fig. S2 DSC curve of pure DES.

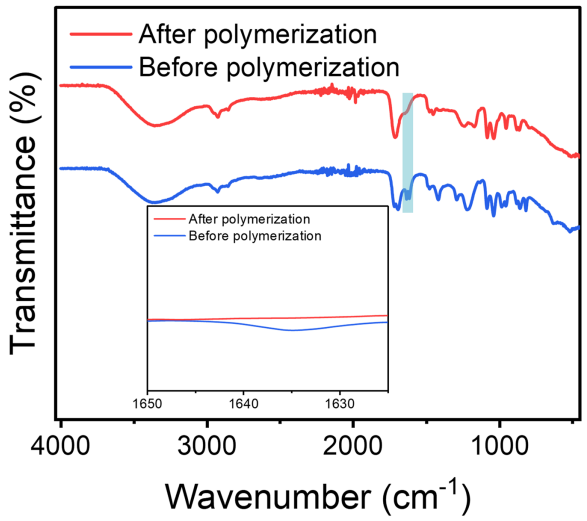

Fig. S3 FTIR spectra of the precursor of PAL before and after polymerization. The inset shows the disappearance of the peak corresponding to the vinyl group.

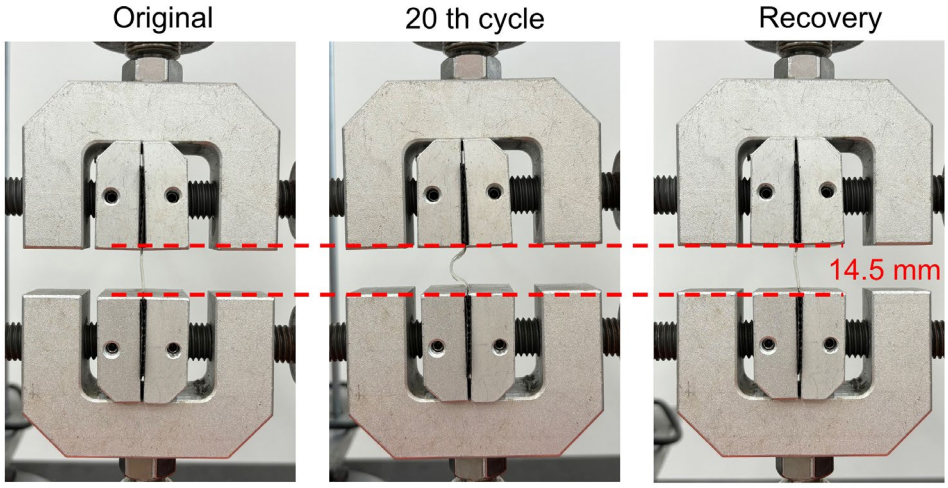

Fig. S4 Cyclic tensile photographs of PAL66 eutectogel.

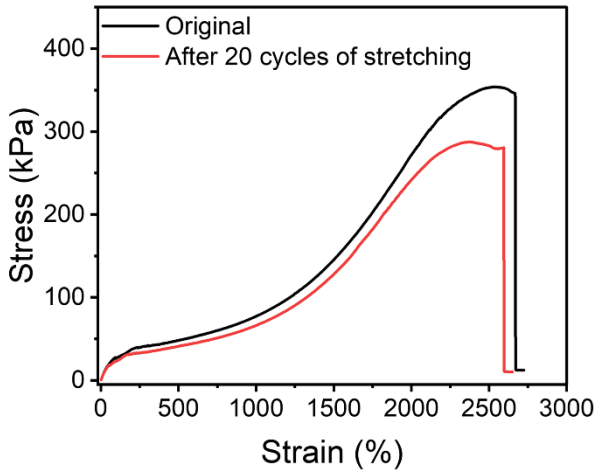

Fig. S5 Stress-strain curve of PAL66 eutectogel after 20 cycles of stretching.

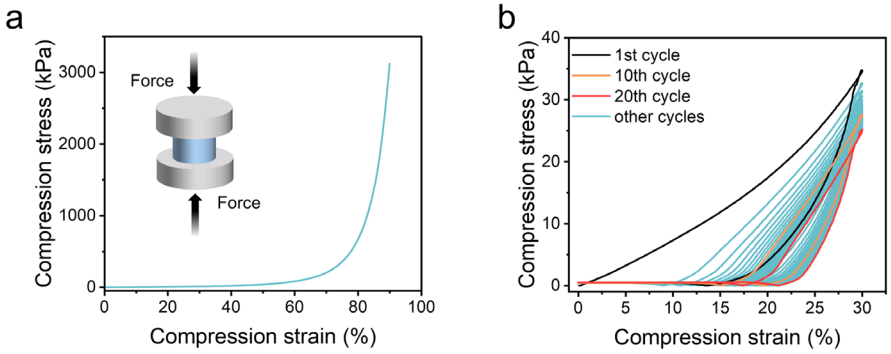

Fig. S6 PAL66 eutectogel compression performance (a) Compression stress-strain curve of PAL66 eutectogel. (b) Performance of PAL66 eutectogel in a 30% strain 20 cycles loading-unloading compression test.

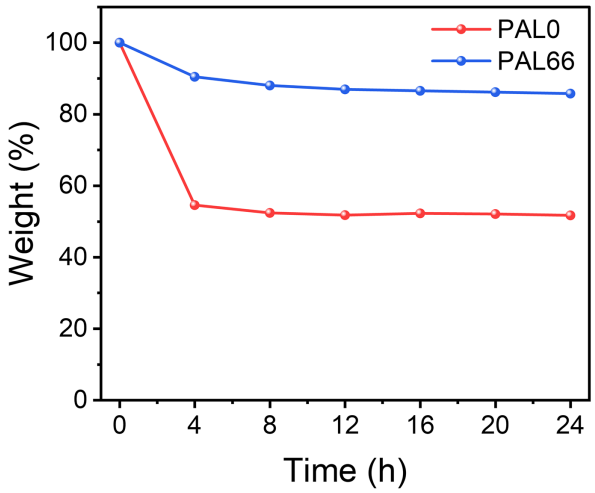

Fig. S7 The mass retention rate of gels.

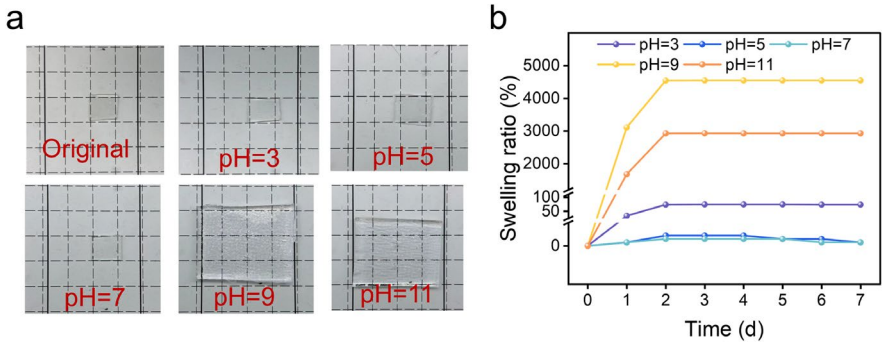

Fig. S8 Swelling behavior in solutions with different pH values. (a) Images of PAL66 immersed in solutions for 7 days. (b) Swelling ratio versus time.

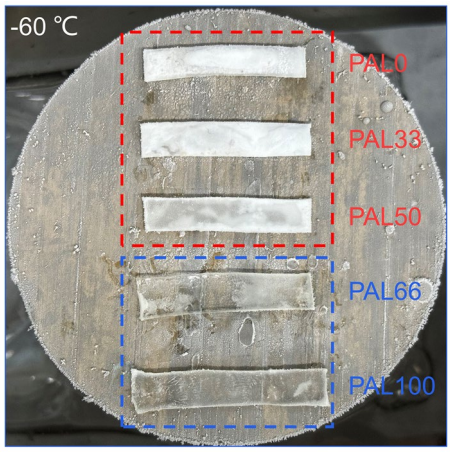

Fig. S9 Photograph of PAL eutectogels at -60 ºC.

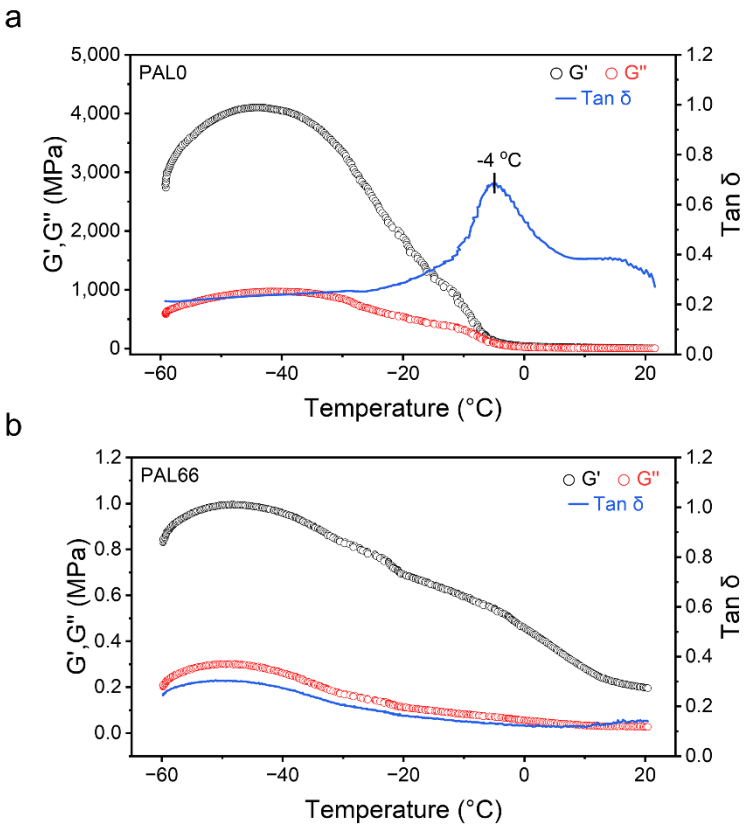

Fig. S10 Storage modulus (G′), loss modulus (G″), and loss angle tangent (Tan δ). (a) PAL0 eutectogel. (b) PAL66 eutectogel.

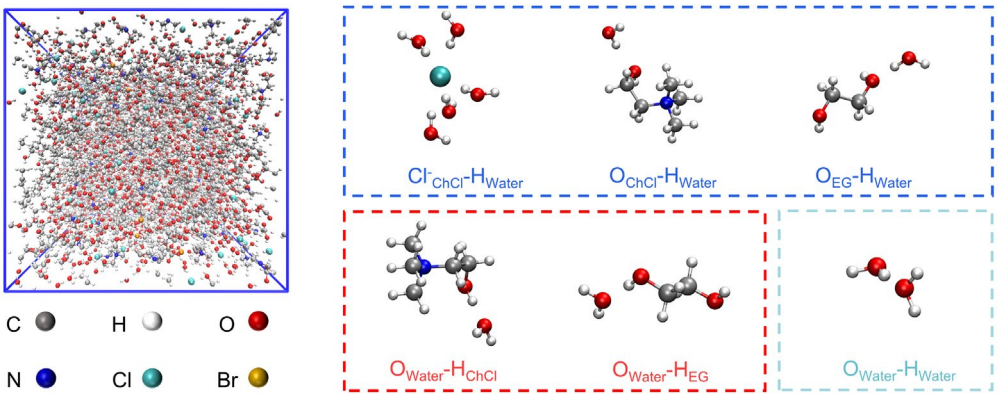

Fig. S11 Snapshots of molecular dynamics simulations of PAL66 eutectogel.

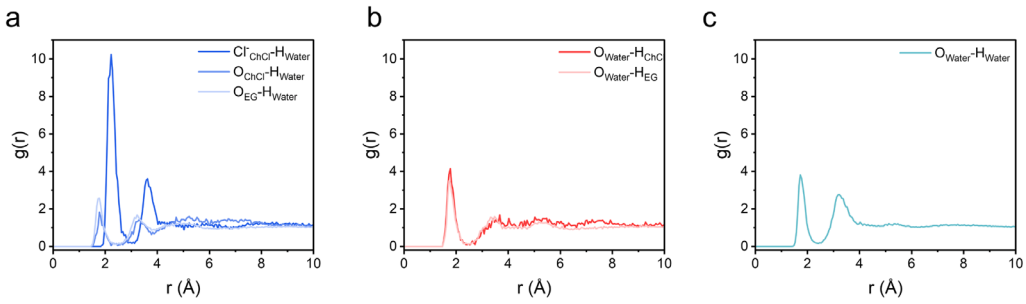

Fig. S12 Plot of the radial distribution function. (a) The radial distribution function of Cl, O in choline chloride, O in ethylene glycol and H in water molecules. (b) The radial distribution function of O in water molecules with H in choline chloride and H in ethylene glycol. (c) The radial distribution function of O in water molecules and H in water molecules.

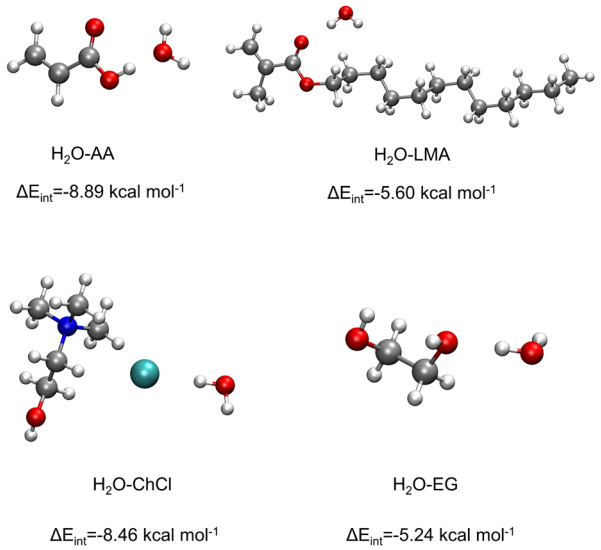

Fig. S13 The binding energy between the different components of the eutectogel.

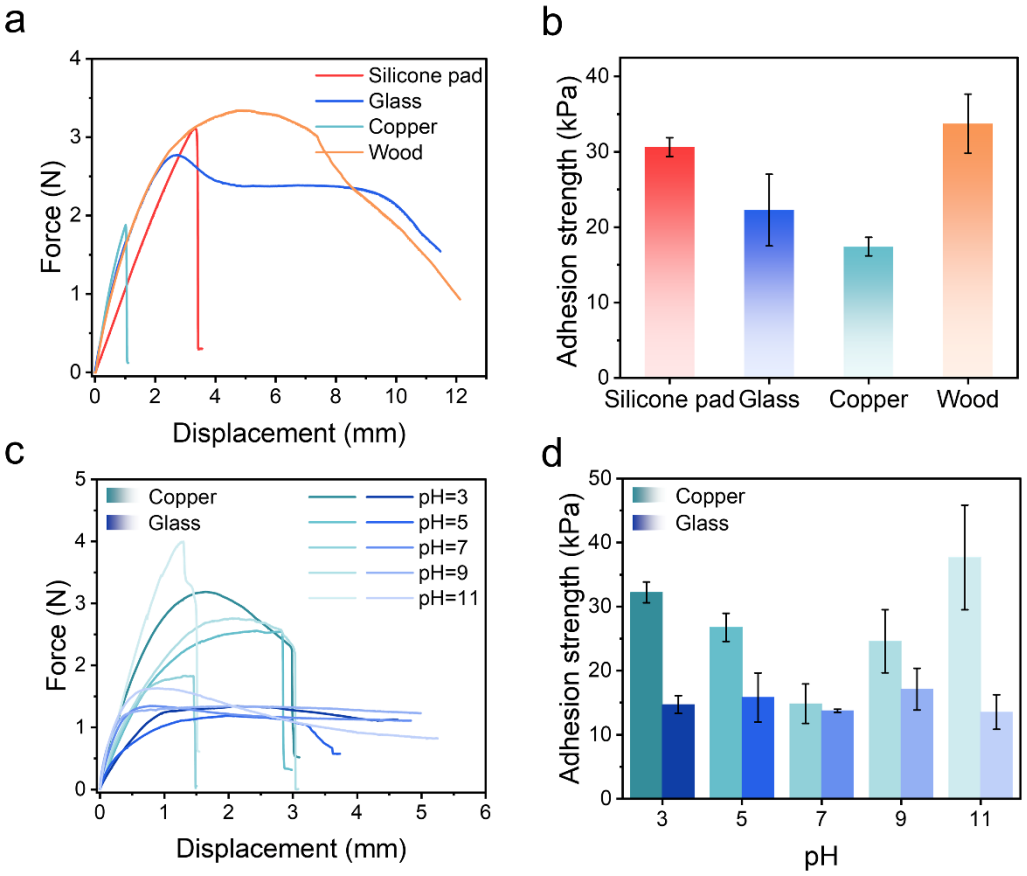

Fig. S14 Adhesion performance in high humidity environments and varying pH levels. (a) Adhesion force curves using different substrates at high humidity (25 ºC, 90% relative humidity. (b) Adhesion strength between PAL66 and different substrates at high humidity (25 ºC, 90% relative humidity). (c) Adhesion force curves using different

substrates at varying pH levels. (pH = 3, 5, 7, 9, 11). (d) Adhesion strength between PAL66 and different substrates at varying pH levels. (pH = 3, 5, 7, 9, 11).

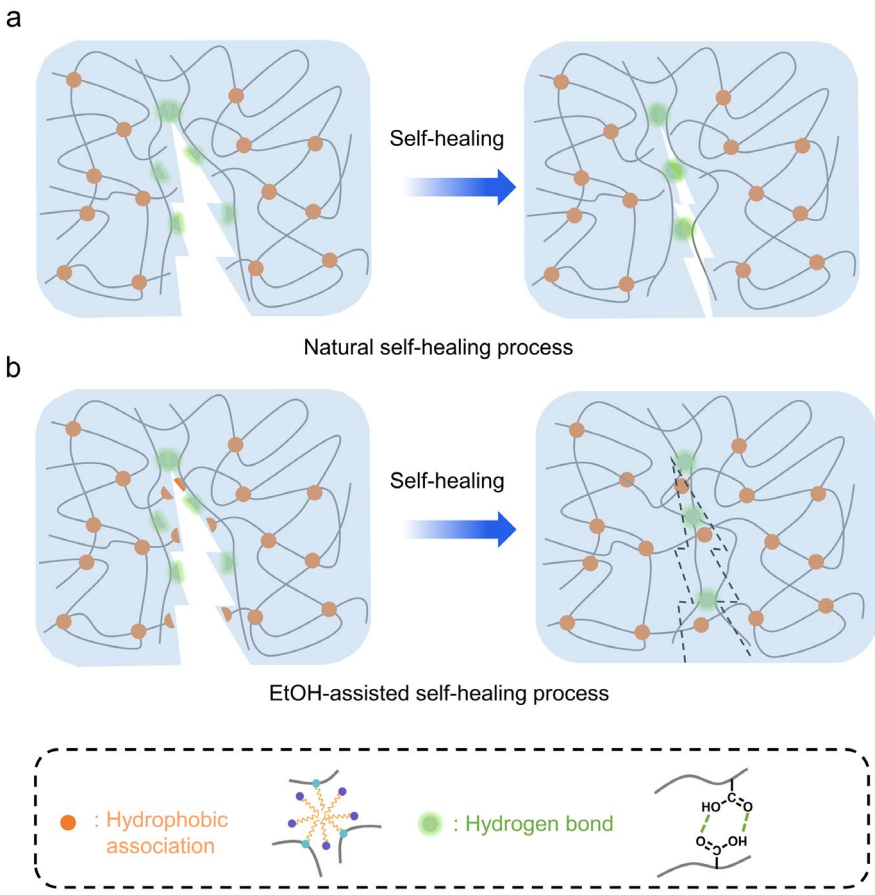

Fig. S15 Schematic representation of the self-healing mechanism of eutectogels. (a) Micro-mechanisms of natural self-healing processes. (b) Micro-mechanisms of EtOH-assisted self-healing process.

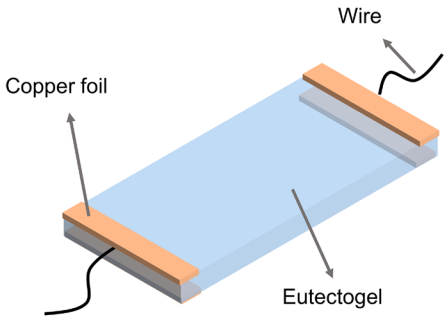

Fig. S16 Schematic illustration of the PAL66 eutectogel-based strain sensor.

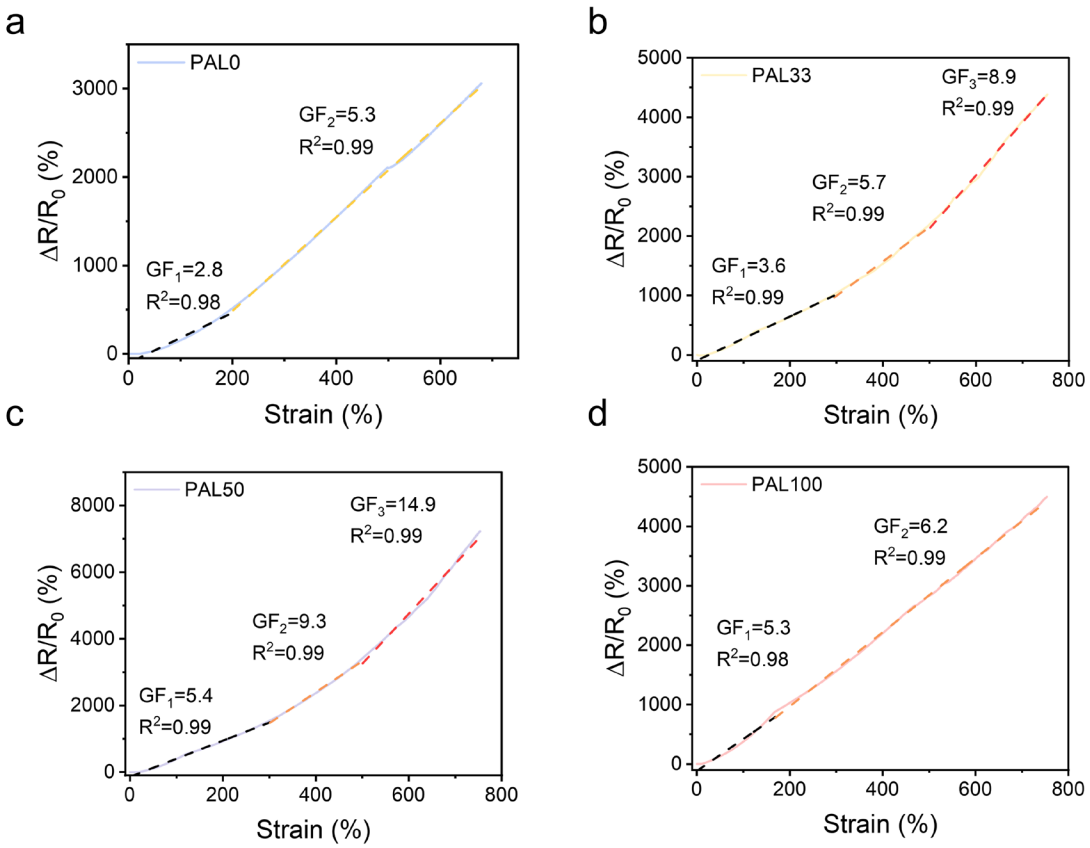

Fig. S17 Relative resistance versus strain curve of PAL eutectogels strain sensors. (a) Relative resistance versus strain curve of PAL0 eutectogel strain sensors. (b) Relative resistance versus strain curve of PAL33 eutectogel strain sensors. (c) Relative resistance versus strain curve of PAL50 eutectogel strain sensors. (d) Relative resistance versus strain curve of PAL100 eutectogel strain sensors.

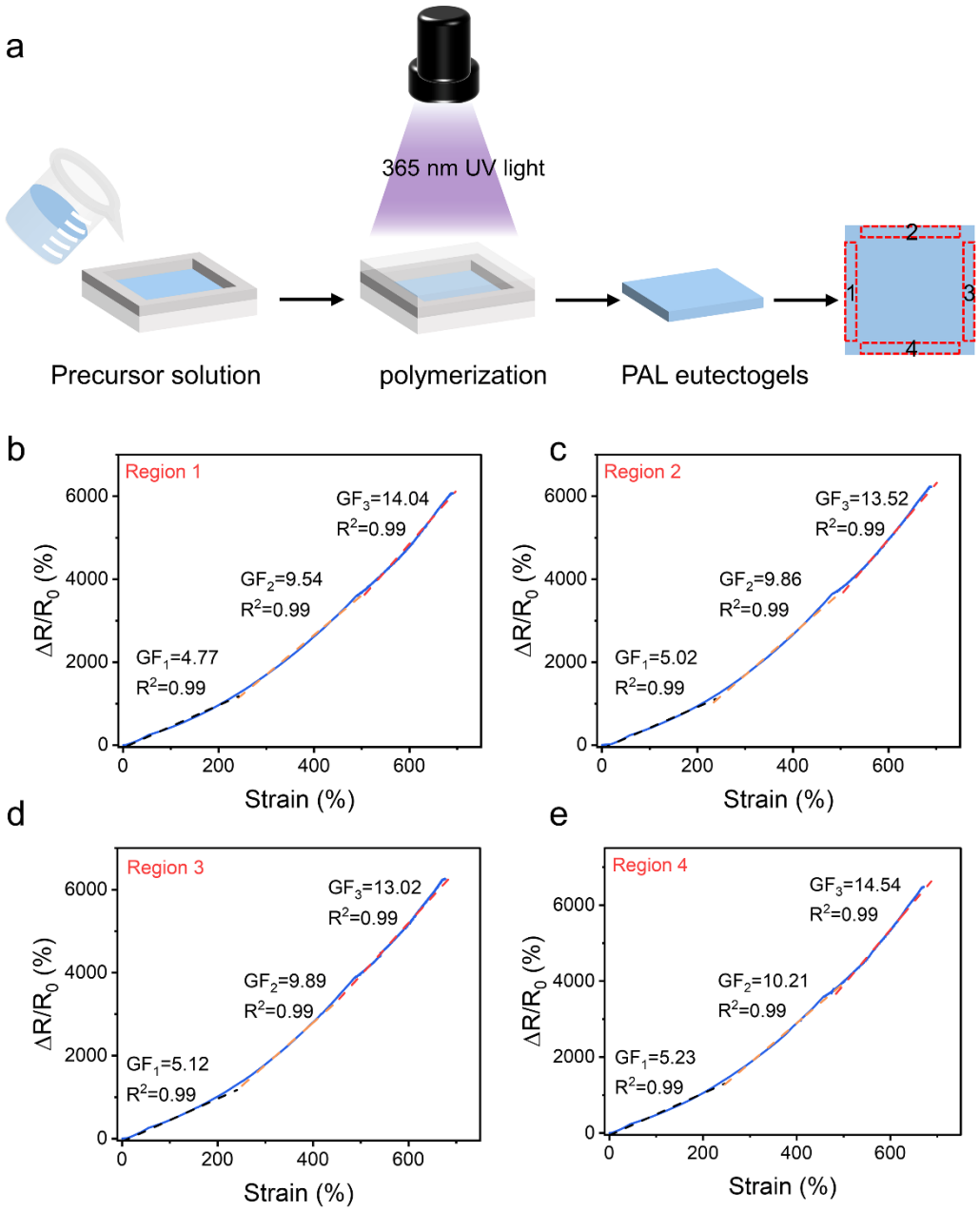

Fig. S18 Reproducibility study of sensing performance. (a) Preparation process of PAL66 eutectogel (b) Relative resistance versus strain curve of region 1. (c) Relative resistance versus strain curve of region 2. (d) Relative resistance versus strain curve of region 3. (e) Relative resistance versus strain curve of region 4.

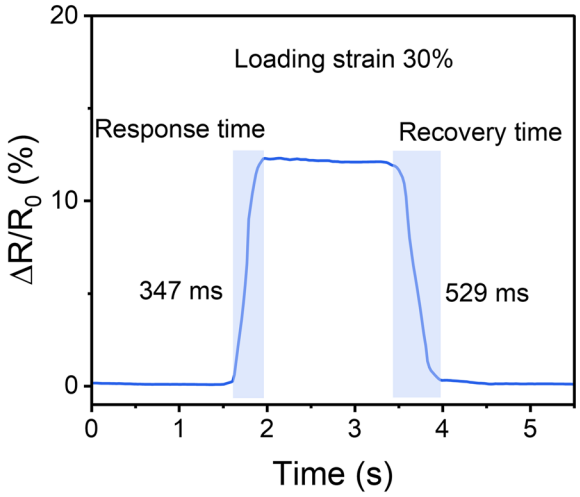

Fig. S19 Response time and recovery time of the PAL66 eutectogel-based strain sensor.

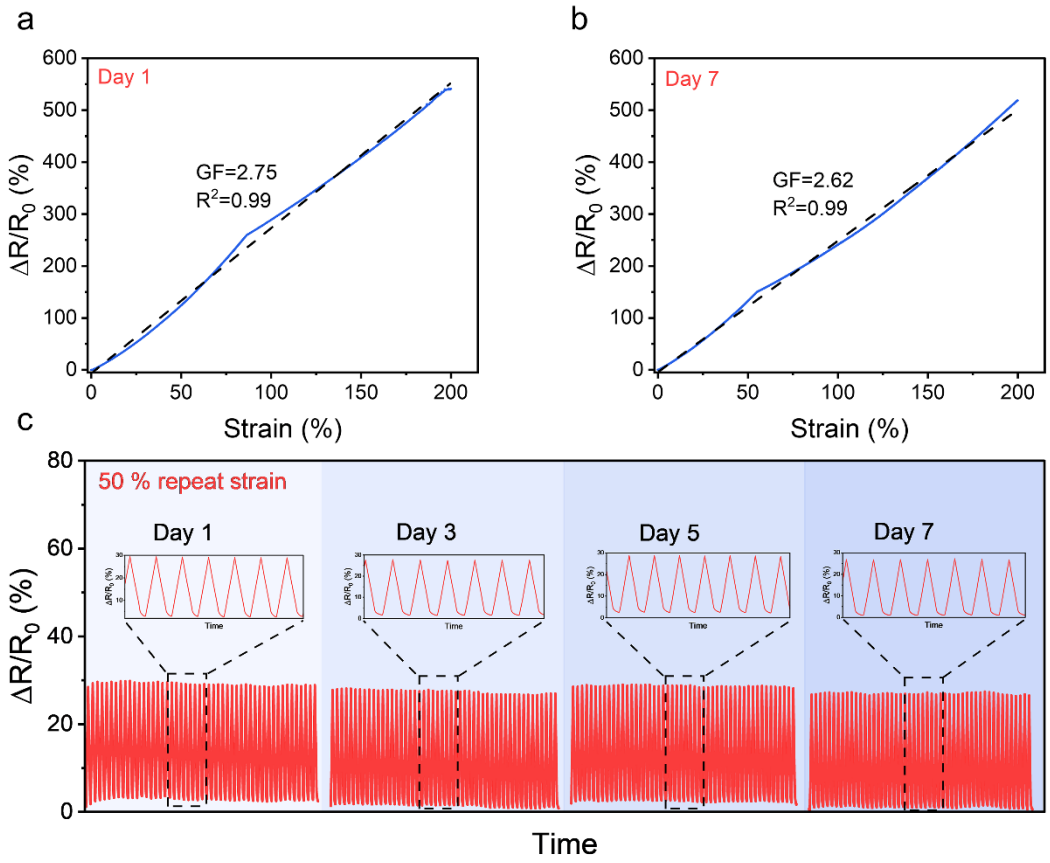

Fig. S20 PAL66 strain sensor long-term stability study. (a) Relative resistance versus strain curves for 200% stretching on Day 1. (b) Relative resistance versus strain curves for 200% stretching on Day 7. (c) Relative resistance versus strain curves for 50% repeat loading-unloading on days 1, 3, 5, and 7.

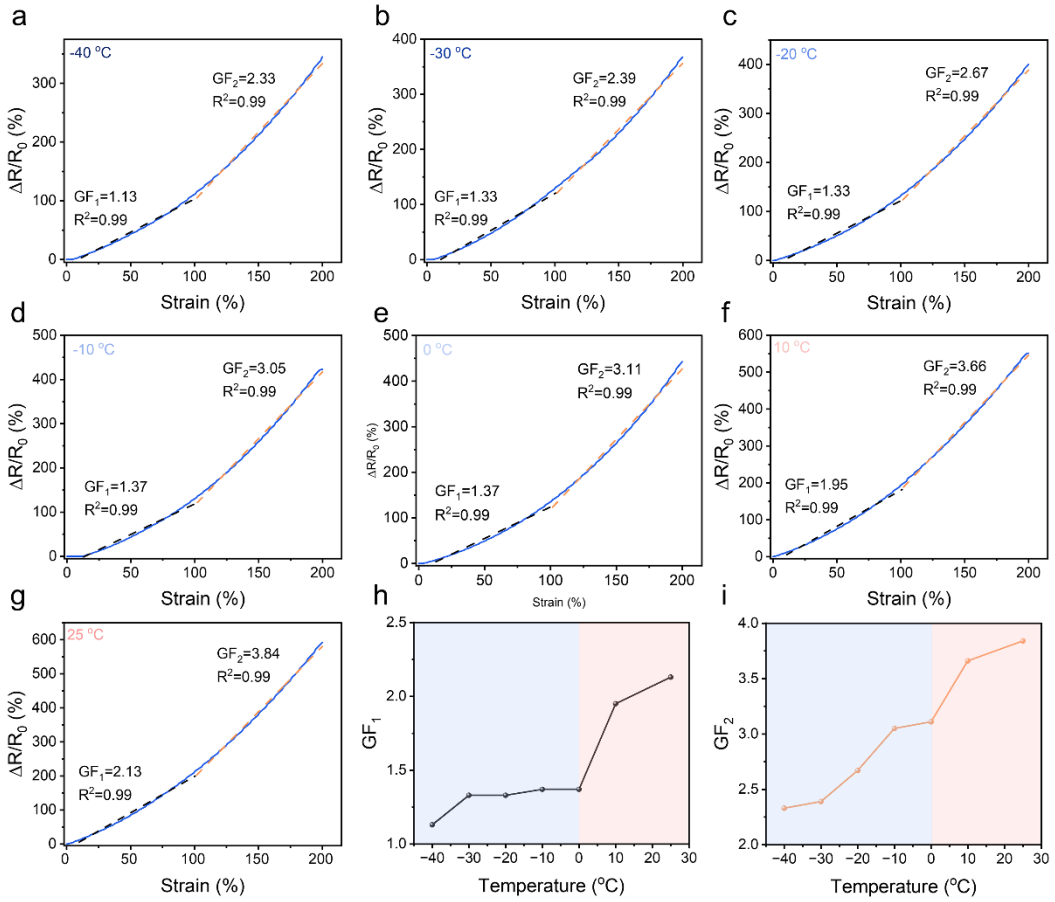

Fig. S21 Relative resistance versus strain curves for 200% strain at different temperatures. (a) Relative resistance versus strain curve at -40 °C. (b) Relative resistance versus strain curve at -30 °C. (c) Relative resistance versus strain curve at -20 °C. (d) Relative resistance versus strain curve at -10 °C. (e) Relative resistance versus strain curve at 0 °C. (f) Relative resistance versus strain curve at 10 °C. (g) Relative resistance versus strain curve at 25 °C (h) GF value versus temperature for 0-100% strain. (i) GF value versus temperature for 100-200%.

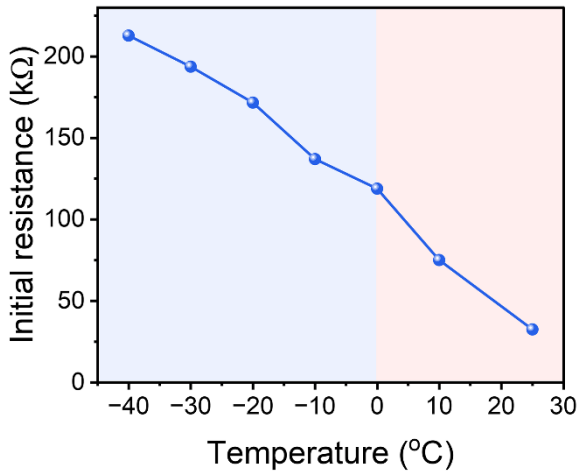

Fig. S22 Initial resistance of PAL66 versus temperature.

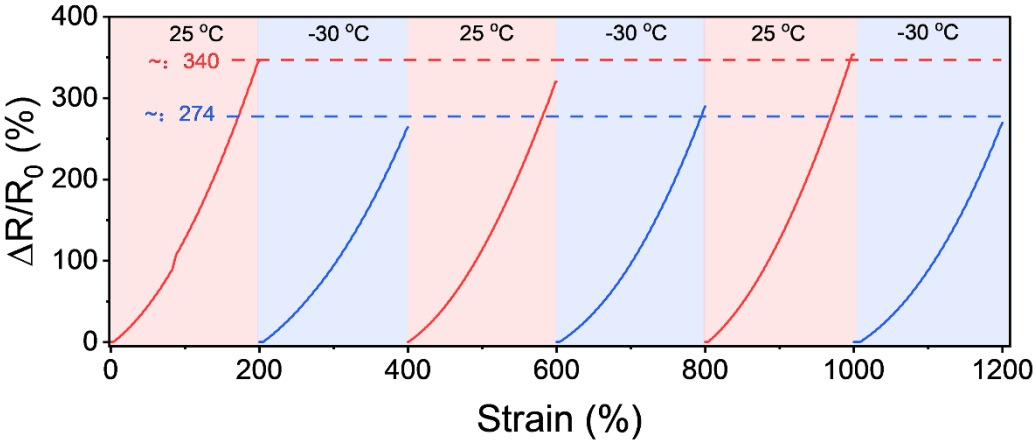

Fig. S23 Relative resistance versus strain at fluctuating temperatures.

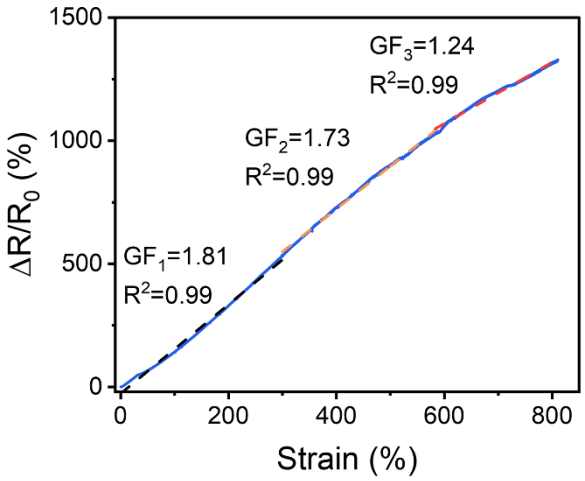

Fig. S24 Relative resistance versus strain curves after drying for 12 h at 25 ºC and 30% relative humidity.

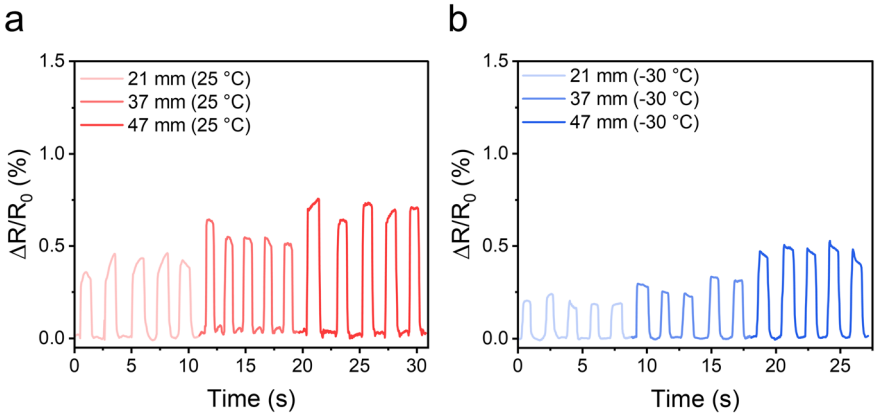

Fig. S25 Strain sensors monitor the degree of bending of mechanical claw-gripping objects of different sizes. (a) Mechanical claw grips objects of different diameters at 25 ºC. (b) Mechanical claw grips objects of different diameters at -30 ºC.

Table S1. Component ratios and nomenclature of PAL eutectogels

Sample	AA (g)	LMA (g)	CTAB (g)	Irgacure 2959 (mg)	DES (g)	H_2O (g)
PAL0	1.5	0.15	0.35	8.25	0	3
PAL33	1.5	0.15	0.35	8.25	1	2
PAL50	1.5	0.15	0.35	8.25	1.5	1.5
PAL66	1.5	0.15	0.35	8.25	2	1
PAL100	1.5	0.15	0.35	8.25	3	0

Table S2. Summary of 6 h and 12 h self-healing efficiencies for PAL66 eutectogel

	Natural self-healing		EtOH assisted self-healing	
	25 ºC	-30 ºC	25 ºC	-30 ºC
6 h	17.39%	8.42%	29.58%	26.94%
12 h	18.19%	9.12%	34.31%	31.77%